Probabilistic Modeling of Shear-Induced Formation and Breakage of Doublets Cross-Linked by Receptor-Ligand Bonds

Mian Long,* Harry L. Goldsmith,# David F.J. Tees,§ and Cheng Zhu*

*George W. Woodruff School of Mechanical Engineering, Georgia Institute of Technology, Atlanta, Georgia 30332-0405, USA; #McGill University Medical Clinic, Montreal General Hospital Research Institute, Montreal, Quebec H3G 1A4, Canada; and §Department of Chemical Engineering and Institute for Medicine and Engineering, University of Pennsylvania, Philadelphia, Pennsylvania 19104, USA

ABSTRACT A model was constructed to describe previously published experiments of shear-induced formation and breakage of doublets of red cells and of latexes cross-linked by receptor-ligand bonds (Tees et al. 1993. *Biophys. J.* 65:1318–1334; Tees and Goldsmith. 1996. *Biophys. J.* 71:1102–1114; Kwong et al. 1996. *Biophys. J.* 71:1115–1122). The model, based on McQuarrie's master equations (1963. *J. Phys. Chem.* 38:433–436), provides unifying treatments for three distinctive time periods in the experiments of particles in a Couette flow in which a doublet undergoes 1) formation upon two-body collision between singlets; 2) evolution of bonds at low shear rate; and 3) break-up at high shear rate. Neglecting the applied force at low shear rate, the probability of forming a doublet per collision as well as the evolution of probability distribution of bonds in a preformed doublet were solved analytically and found to be in quite good agreement with measurements. At high shear rate with significant force acting to accelerate bond dissociation, the predictions for break-up of doublets were obtained numerically and compared well with data in both individual and population studies. These comparisons enabled bond kinetic parameters for three types of particles cross-linked by two receptor-ligand systems to be calculated, which agreed well with those computed from Monte Carlo simulations. This work can be extended to analyze kinetics of receptor-ligand binding in cell aggregates, such as those of neutrophils and platelets in the circulation.

GLOSSARY

a	bond interaction parameter (in nm)
A_c	contact area (in μm^2)
B_i	renormalization factor
C	orbit constant (given by Eq. A10)
C_f, $\langle C_f \rangle$	angle factor ($= \sin^2\theta_1 \sin 2\phi_1$), mean value
D	empirical parameter (given by Eq. 19; in μm^{-4} nM^{-q})
f_c, f_p	two-body collision frequency per particle, capture value (in s^{-1})
F	applied force (Eq. 3)
F_N, F_S	hydrodynamic normal and tangential forces, respectively (given by Eqs. 1 and 2; in pN)
$F_{N,max}$, $\langle F_{N,max} \rangle$	maximum normal force in a force cycle, mean value (in pN)
$g(x, t)$, $g_m(x, t)$	probability-generating function, conditioned by assuming there are m bonds initially
G	shear rate (in s^{-1})
h	minimum distance of approach between sphere surfaces (in nm)
$H_c, H_p, \bar{H}_p$	total two-body collision frequency per unit volume, capture value, weighted time average of H_p (in $s^{-1} \cdot \mu l^{-1}$)
i	number of half-rotations
$J(u)$, $J_m(u)$	arbitrary integration function, conditioned by assuming there are m bonds initially
$k_f^{(n)}, k_f, k_f^L, k_f^H, k_f^M$	forward rate coefficient per unit density for the formation of the nth bond, constant value, values derived from fitting data from the low and high shear rate periods as well as combined both periods (in $\mu m^2 \cdot s^{-1}$)
$k_r, k_r^{(n)}, k_r^0$	reverse rate coefficient, value for the dissociation of the nth bond, value at zero force (in s^{-1})
k_B	Boltzmann constant ($= 1.38 \times 10^{-2}$ nm · pN · K^{-1})
m_r, m_l, m_{min}	number densities of receptors and ligands, minimum value of the two (in μm^{-2})
M_r, M_l, M_b, M_w	molecular species of receptor, ligand and bond, respectively, molecular weight
n, $\langle n \rangle$	number of bonds, mean value at $t = t_2$
N	number of samples or data points
N_f	number of fitting parameters

Received for publication 23 January 1998 and in final form 20 September 1998.

Address reprint requests to Dr. Cheng Zhu, School of Mechanical Engineering, Georgia Institute of Technology, Atlanta, GA 30322-0363. Tel.: 404-894-3269; Fax: 404-894-2291; E-mail: cheng.zhu@me.gatech.edu.

Dr. Long is on leave from the Bioengineering Institute, Chongqing University, Chongqing 400044, People's Republic of China.

0006-3495/99/02/1112/17 $2.00

N_i number of measurements comprising the ith data point
N_S number density of singlets in particle suspension (in μl^{-1})
p_b, p_f probability of bond breakage and formation in time Δt, respectively (given by Eq. 4)
p_n, $p_{n|m}$ probability of having n bonds ($= 0, 1, 2 \ldots$), conditioned by assuming that there are m bonds initially
p_+, p_- random number obeying a uniform distribution in (0, 1)
$P(\cdot)$ probability of the argument
P_a probability of adhesion per two-body collision
q dimensionless empirical parameter (given by Eq. 19)
r polar coordinate (in μm)
r_e equivalent axis ratio of doublet ($= 1.98$)
R sphere radius (in μm)
$\hat{s}_i$ predicted standard error
t, t_1, t_2, t_f arbitrary time, lifetime of a collision doublet or contact duration of two-body collision, end time of the low shear rate phase, time scale for the formation of an additional bond in a preformed doublet (in s)
T absolute temperature (in K)
u argument of arbitrary integration function $J(u)$
u_j sphere velocity relative to the reference sphere along X_j axis; $u_1 = u_2 = 0$, $u_3 = GX_2$ (in $\mu m \cdot s^{-1}$)
x, x_i argument of probability-generating function $g(x, t)$, of function $y(x_i)$
X_j Cartesian coordinates with origin at the center of the reference sphere in a simple shear field; $j = 1$ is the vorticity axis, $j = 2$ is the direction of velocity gradient, and $j = 3$ is the direction of flow (in μm)
y_i, $y(x_i)$ measurement and prediction at x_i, respectively

Greek symbols

α_N, α_S force coefficients (Eqs. 1 and 2)
δ_{nm} Kronecker delta symbol
ϵ, $\bar{\epsilon}$ two-body collision capture efficiency, weighted time average
Δt incremental time step
η suspending medium viscosity (in Poise)
θ_1, ϕ_1 polar and azimuthal angles of doublet axis with respect to the vorticity axis (X_1) as the polar axis
θ_2 polar angle of doublet major axis with respect to X_2 axis as the polar axis
σ_i, $\hat{\sigma}_i$, σ_n standard deviation, predicted value, value of probability distribution of initial bonds
τ end point of contact duration at low shear rate (in s)
χ^2, χ^2_v chi square statistic, reduced value ($=\chi^2/\nu$)
ν number of degrees of freedom ($= N - N_f$)
ν_r, ν_l, ν_b stoichiometric coefficient of receptor, ligand and bond, respectively (given by Eq. 17)

INTRODUCTION

This paper deals with modeling the formation and break-up of receptor-ligand bonds in sheared suspensions, a subject of considerable importance in the circulation, where formation and break-up of blood cell aggregates occur in a variety of physiological and pathological conditions. Thus, nonpathogenic neutrophil aggregation is thought to be important in the vicinity of tissue damage (Hill, 1987). Agonist-induced platelet aggregation plays a key role in the growth of thrombi on vessel walls, and platelets also aggregate with metastatic tumor cells (Honn et al., 1992), which themselves are known to form aggregates (Weiss et al., 1988).

To model the biophysics of cell aggregation in a shear field is challenging because of the coupling between the hydrodynamics of the cell suspension and the chemical kinetics of the receptor-ligand binding, the latter governing the dynamic changes in bond number during the interaction. When two cells first aggregate upon colliding in a shear field, they are likely linked by only a single bond. This bond can either break, leading to break-up of the doublet, or the number of bonds can grow (albeit nonmonotonically) until dissociation equals formation and a dynamic equilibrium bond number is reached. Further changes in the bond number require a change in external conditions (such as hydrodynamic forces) or in the expression and activation of adhesion molecules. Thus, L-selectin shedding and subsequent β_2-integrin activation have been shown to influence neutrophil aggregation in shear flow (Taylor et al., 1996).

The present paper focuses on the effect of hydrodynamic force on the members of an aggregate and hence the bonds holding it together. These forces can be quite complex, even in the simplest of cases. For example, the following expressions have been derived for the normal force (F_N) acting along and the shear force (F_S) acting normal to the major axis of a doublet of rigid spheres (e.g., a doublet of aggregating neutrophils) in simple shear flow (Tha and Goldsmith, 1986):

$$F_N = \alpha_N(h)\, \eta\, GR^2 \sin^2\theta_1 \sin 2\phi_1, \qquad (1)$$

$$F_S = \alpha_S(h)\,\eta\,GR^2 \sin\theta_1 \left\{\frac{(2\sin^2\theta_1\cos^2\phi_1 - 1)^2\sin^2\phi_1 + \cos^2\theta_1\cos^2\phi_1}{1 - \sin^2\theta_1\cos^2\phi_1}\right\}^{1/2}, \quad (2)$$

where η is the suspending medium viscosity, G is the shear rate, R is the sphere radius, and θ_1 and ϕ_1 are the azimuthal and polar angles describing the orientation of the doublet axis with respect to the vorticity axis X_1 of the shear field (see Fig. 2 below); α_N and α_S are force coefficients that are weakly dependent on the distance, h, between sphere surfaces (see the Glossary).

How these hydrodynamic forces are distributed among the bonds depends on the distribution of bonds within the contact area. If the cells in the aggregate can flatten and form large contact areas, bonds at the circumference of the contact area will carry most of the stress, whereas those on the inside will be largely unstressed. For small contact areas or low bond densities, however, the situation is different. A small number of bonds (say, three or four) will likely split the force equally, but should one dissociate, those remaining will feel a large increase in the force per bond.

A likely effect of external force on the bonds is to accelerate their dissociation. Twenty years ago, George Bell (1978) formulated such an effect as an exponential force dependence of the reverse rate coefficient:

$$k_r^{(n)}(F/n) = k_r^0 \exp[aF(t)/nk_BT], \quad (3)$$

where k_r^0 is the zero-force reverse rate constant, a is the bond interaction parameter, $F(t)$ is the force (for doublet rotation in shear flow, a periodic function of time) shared among n bonds, k_B is the Boltzmann constant, and T is the absolute temperature. Other expressions for the force dependence of kinetic rates have also been proposed (Dembo et al., 1988; Evans et al., 1991). A major effort in the field is to determine the appropriateness of these expressions and the associated parameters (Evans and Ritchie, 1997; Piper et al., 1998); the present paper contributes in this regard.

Theoretical and experimental models are needed to understand aggregation and disaggregation in the presence of such dynamically changing applied forces and bond numbers. In vitro assays are useful in this connection, because it is possible to control shear profile (e.g., using a flow chamber) and biochemistry (e.g., using molecules attached to latex beads). Relevant assays include homotypic neutrophil aggregation in a flow cytometer (Simon et al., 1990), platelet aggregation in tube flow (Bell et al., 1989a,b, 1990), and the break-up of doublets of sphered red cells (Tha et al., 1986; Tees et al., 1993) in Poiseuille flow. More recently, the latter technique was extended to study formation and breakage of doublets of sphered red cells and latex beads in Couette flow in a cone-and-plate rheoscope (Tees et al., 1993; Tees and Goldsmith, 1996; Kwong et al., 1996).

One method for modeling the shear-induced break-up of cell aggregates is to use Monte Carlo simulation to track the number of bonds under stress (Hammer and Apte, 1992; Tees et al., 1993). In this approach, the initial number of bonds, n, cross-linking the cells is randomly chosen from a Poisson distribution with a preset average number of bonds. Time is divided into discrete steps of length Δt. In each time step, the forces acting on the bonds are calculated. The probability of bond breakage, p_b, is given by (Hammer and Apte, 1992)

$$\begin{aligned} p_b &= 1 - \exp(-k_r^{(n)}\Delta t) \\ &= 1 - \exp\{-k_r^0 \exp[aF(t)/nk_BT]\Delta t\}, \end{aligned} \quad (4a)$$

where Eq. 3 has been used to expand the reverse reaction rate. Furthermore, it can be postulated that the probability of adding a new bond to a doublet is given by

$$p_f = \Delta t/t_f, \quad (4b)$$

where t_f is the time scale for the formation of an additional bond in an existing doublet. A cycle of force calculation, bond formation, and break-up testing is continued until "break-up" for a series of simulated doublets. The resulting time distribution of break-up can be compared to experimental results to determine parameters for models of force dependence of reaction rates. The Monte Carlo simulation was used in the previous studies from one of our laboratories (Tees et al., 1993; Tees and Goldsmith, 1996; Kwong et al., 1996), because it was thought that forces were too complex to be solved using a closed-form computation with a dynamically changing bond number. The present paper demonstrates, however, that it is indeed possible to directly model the time-varying distributions of bonds despite the formidable expressions for the force loading.

This alternative approach is the probabilistic method recently developed by the other of our laboratories (Piper et al., 1998; Piper, 1997; Chesla et al., 1998; Zhu and Chesla, 1997; Long and Zhu, 1997). In contrast to the Monte Carlo approach, which simulates the fate of a series of bonds to generate an ensemble of realizations from which statistics are obtained, the present method solves the corresponding probabilistic variables directly from a set of master equations (McQuarrie, 1963), which describe the binding kinetics of a small number of receptors and ligands:

$$\begin{aligned} \frac{dp_n}{dt} &= A_c m_r m_l k_f^{(n)} p_{n-1} - (A_c m_r m_l k_f^{(n+1)} + nk_r^{(n)})p_n \\ &\quad + (n+1)k_r^{(n+1)} p_{n+1}. \end{aligned} \quad (5)$$

Here, p_n is the probability of having n bonds at time t, and m_r and m_l are the respective number densities of receptor and ligand. An assumption employed by Eq. 5, which simplified the original form of McQuarrie's (1963) equations, was that the number of receptors and ligands in the contact area, A_c, greatly exceeds the number of bonds that have nonvanishing probabilities. Consequently, the forward rate coefficient per unit density, $k_f^{(n)}$ (in $\mu m^2\ s^{-1}$), appears in Eq. 5 as a lumped per-cell forward rate coefficient, $A_c m_r m_l k_f^{(n)}$ (in s^{-1}). Another modification to McQuarrie's master equations, first introduced by Cozens-Roberts et al. (1990), was

to make the reverse rate coefficient, $k_r^{(n)}$, a function of the applied force, $F(t)$, and the number of bonds, n, that shared the force (Eq. 3). Note that k_r in the second term on the right-hand side of Eq. 5 should be different from the one in the last term, as the former was the reverse rate coefficient for the n bond state, whereas the latter was that for the $(n + 1)$ bond state (as indicated by their respective superscripts). In contrast, the forward rate coefficient is assumed to be constant, $k_f^{(n)} = k_f$, independent of bond number n in the present work. This simplification has been assumed by several groups, including ourselves (Hammer and Lauffenburger, 1987; Tees et al., 1993), although it has not been tested experimentally, and a more general expression may be needed for future work.

McQuarrie's (1963) work has formally established the master equations as a well-founded generalization of the deterministic kinetic equation suitable for small systems (see also Chesla et al., 1998; Zhu et al., 1998). In Appendix B, the Monte Carlo approach is shown to be mathematically equivalent to a finite-difference approximation of the master equations, thereby putting it on an equally rigorous theoretical footing. One incidental, but important, advantage of the master equations is that the computational cost is significantly less than for the Monte Carlo approach. This allowed us to explore the effect of relaxing many of the simplifying assumptions employed in previous work.

In previous work, only doublet break-up at high shear rate was treated by Monte Carlo simulations. In the present paper, by comparison, all three separate time periods in the experiments have been modeled using the same set of master equations. The three time periods are 1) the encounter period of the shear-induced two-body collision during which the first bond may be formed; 2) the low shear rate period (for a given doublet, this period starts after the formation of the first bond) during which the bond number may grow; and 3) the high shear rate period during which the doublet may break up. The analysis of the first phase enabled us to derive an expression for the collision capture efficiency. Previously, this was either assumed a priori as an empirical parameter (Bell et al., 1989a,b, 1990; Huang and Hellums, 1993a–c) or calculated from a deterministic kinetic criterion (Bell, 1981; Tandon and Diamond, 1997). The analysis of the second phase allowed us to introduce the time-averaged probabilities of survival and break-up at low shear rate, both of which can be directly compared to experimental measurements.

Our goal here is to offer a unifying theoretical framework to interpret experiments regardless of the loading regime, receptor system, and assay technique used. Such a framework is a requirement for a full understanding of the biophysics of cell adhesion at the fundamental level.

ANALYSIS

The experiments that were modeled consisted of studies of formation and breakage of doublets. The three types of particles and the two kinds of cross-linking molecules used in the experiments are illustrated in Fig. 1. In both cases of individual as well as population studies, doublets were first allowed to form through collisions of two singlets at low shear rate ($\sim 8\ s^{-1}$) in Couette flow within the rheoscope. They were then subjected to a known higher shear rate ($15–145\ s^{-1}$). In studies of individual break-ups with

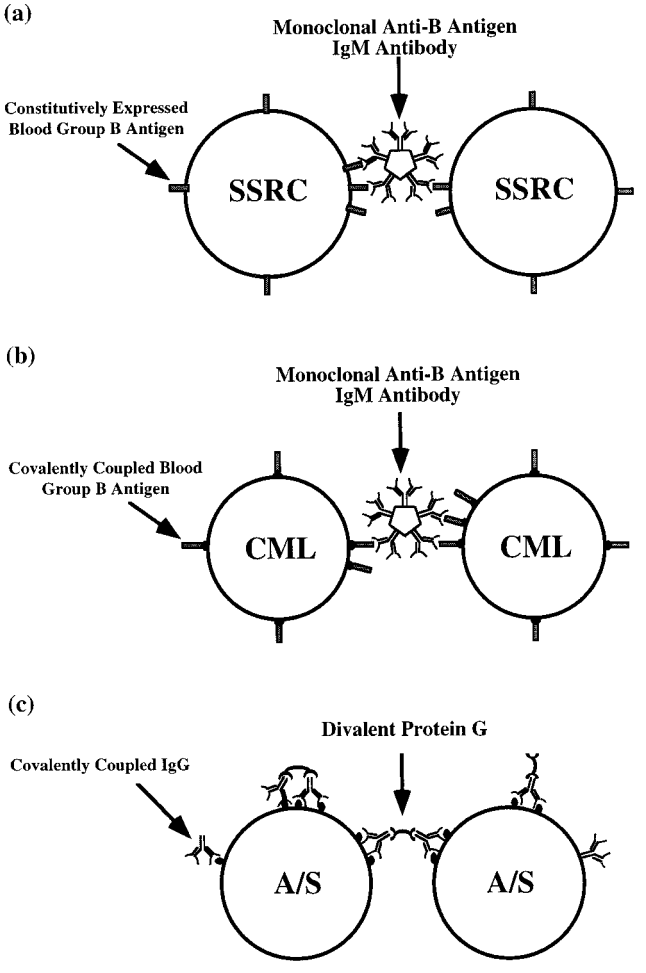

FIGURE 1 Schematic (not to scale) of the three model spherical particles and two cross-linking molecules used in the doublet break-up experiments (Tees et al., 1993; Tees and Goldsmith, 1996; Kwong et al., 1996). (*a*) Sphered and swollen red cells (SSRCs) expressing blood group B antigen cross-linked by monoclonal anti-B antigen IgM antibody. The estimated contact area (based on an estimated 20-nm separation between the cell surfaces) and site densities of B antigen and IgM antibody are $\sim 0.25\ \mu m^2$, $\sim 8 \times 10^3\ \mu m^{-2}$, and $\sim 60\ \mu m^{-2}$, respectively (Tees et al., 1993). (*b*) Carboxyl-modified latex (CML) spheres covalently coupled with synthetic blood group B antigen cross-linked by monoclonal anti-B antigen IgM antibody. The estimated contact area and site densities of B antigen and IgM antibody are $\sim 0.25\ \mu m^2$, $\sim 4 \times 10^5\ \mu m^{-2}$, and $\sim 34\ \mu m^{-2}$, respectively (Tees and Goldsmith, 1996). (*c*) Aldehyde/sulfate (A/S) latex spheres covalently coupled with monoclonal IgG antibody cross-linked by 0.9 nM divalent Gamma Bind G (a recombinant fragment of protein G, $M_w = 22{,}000$). The estimated contact area and site density of IgG antibody are $\sim 0.10\ \mu m^2$ and $\sim 240\ \mu m^{-2}$, respectively (Kwong et al., 1996). The Gamma Bind G is present at a fourfold excess in solution over [IgG]. The contact areas for both latex beads were based on an estimated 10-nm separation between bead surfaces.

sphered and swollen red cells (SSRCs) (Tees et al., 1993) carboxyl-modified latexes (CML), and aldehyde/sulfate (A/S) latexes (Tees and Goldsmith, 1996; Kwong et al., 1996), preformed doublets were continuously observed and videotaped until they broke up or were lost from view. In population studies with A/S latexes (Kwong et al., 1996), after being subjected to low shear rate for 30 min, the number of doublets formed per unit volume was counted, and the suspension was then subjected to a high shear rate for known periods of time, after which the number of doublets broken up per unit volume was determined. Accordingly, Eq. 5 was solved for three distinct time periods with appropriate initial and matching conditions to connect the periods.

Formation of doublets upon collision

We first treat the process of doublet formation involving two-body collisions between rigid spheres in Couette flow. Following Smoluchowski (1917), we consider a suspension of uniformly dispersed, equal-sized spheres (singlets) of radius R, whose density (number per unit volume) is N_S, and assume that collisions occur after the rectilinear approach of particles to within a distance $2R$ of their centers. Upon apparent contact, the collision doublet so formed rotates with the angular velocity of a rigid spheroid of axis ratio r_e ($= 1.98$), until the mirror image of the position of apparent contact is reached, when the doublet separates (Goldsmith and Mason, 1967). Fig. 2 shows that a reference sphere placed at the origin of the flow field ($u_3 = GX_2$; $u_1, u_2 = 0$) will collide with all other spheres whose centers pass through a collision disc of radius $2R$ and origin coincident with the reference sphere. Taking cylindrical polar coordinates X_3 (direction of flow), r, and θ_2 with origin at the center of the reference sphere, the elementary number of collisions, $df_c(r, \theta_2)$, occurring per unit time in an area element of the disc, $r\,dr\,d\theta_2$, can be written as

$$df_c(r, \theta_2) = N_S|u_3(r, \theta_2)|r\,dr\,d\theta_2, \tag{6}$$

where $u_3(r, \theta_2) = Gr \sin \theta_2$ is the sphere velocity relative to the reference sphere. Integrating over the entire collision disc ($0 \le r \le 2R$, $-\pi \le \theta_2 \le \pi$) yields the two-body collision frequency *per particle*,

$$f_c = \frac{32}{3} GN_S R^3. \tag{7a}$$

Multiplying Eq. 7a by N_S to account for all singlets in the suspension and dividing by 2 to discount counting of the same singlet twice results in the well-known equation (Smoluchowski, 1917) for the total two-body collision frequency *per unit volume*:

$$H_c = \frac{16}{3} GN_S^2 R^3. \tag{7b}$$

Bell (1981; see also Tandon and Diamond, 1997) introduced the probability of adhesion per collision, P_a, which

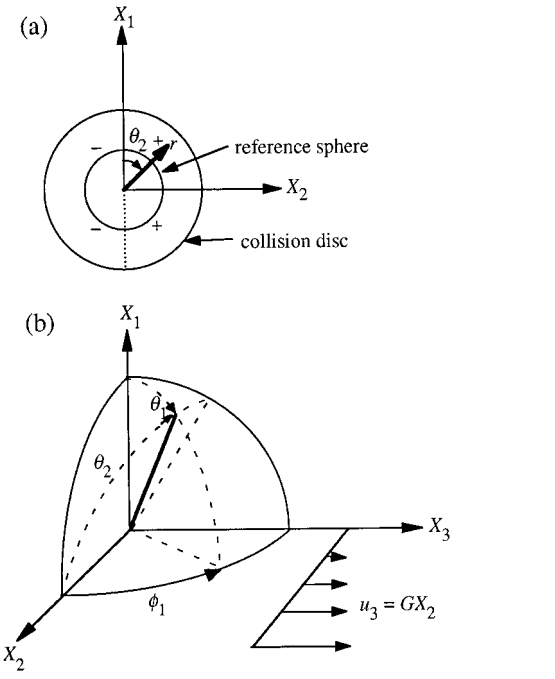

FIGURE 2 Coordinate system describing two-body collisions between rigid spheres of radius R in Couette flow. (*a*) Cylindrical polar coordinates X_2, r, θ_2 showing collision disc of radius $2R$ drawn about the reference sphere, radius R, in the X_1X_2 plane normal to the direction of flow along the X_3 axis. All spheres whose centers lie on a path having $r < R$ are assumed to collide with the reference sphere. The number of collisions is equal on both sides (+) and (−) of the X_1X_2 plane. (*b*) Spherical polar coordinates, ϕ_1, θ_1 with X_1 as the polar and vorticity axis, constructed at the origin of the field of flow.

could take a value of either 0 or 1, based on a deterministic criterion assumed a priori, into the right-hand side of Eq. 6 to obtain the fraction of the elementary number of collisions that results in doublet formation per unit time, df_p.

Our extension of Bell's approach is to solve P_a from Eq. 5 under the condition that there is no bond initially. The result can be expressed by a Poisson distribution (see Appendix A),

$$\begin{aligned} p_n &= \frac{1}{n!}[(A_c m_r m_l k_f/k_r^0)(1 - e^{-k_r^0 t_1})]^n \\ &\quad \cdot \exp[-(A_c m_r m_l k_f/k_r^0)(1 - e^{-k_r^0 t_1})] \qquad (8a) \\ &\approx \frac{1}{n!}[A_c m_r m_l k_f t_1]^n \exp[-A_c m_r m_l k_f t_1] \end{aligned}$$

and

$$P_a = 1 - p_0 \approx A_c m_r m_l k_f t_1. \tag{8b}$$

The approximation for p_n given in Eq. 8a is valid because of the relatively short lifetime, t_1, of a collision doublet (encounter duration of two singlets in the absence of adhesive bonds to cross-link them) even at low shear rate (average value $\langle t_1 \rangle = 5\pi/6G \approx 0.3$ s; Goldsmith and Mason, 1967) compared to the time scale of bond formation ($t_f =$

$(A_c m_r m_l k_f)^{-1} \approx 29$ s (cf. values listed in Table 1)). For the same reason, the force dependence of the reverse rate coefficient should have no effect, as the process is dominated by the forward rate constant. Thus k_r is absent from the approximate solutions given by the far right-hand side of Eq. 8. We also assumed a constant A_c, as we believed this was a better approximation than Bell's (1981) assumption that $A_c \propto (2R)^2 - r^2$, although results were available either way. Multiplying the right-hand side of Eq. 6 with P_a given by Eq. 8b and following the same steps as those used to derive f_c and H_c, the number of doublets formed in unit time (instantaneous two-body collision capture frequency) *per particle*, f_p, and the corresponding total number *per unit volume*, H_p, can be obtained as

$$H_p = \frac{N_S}{2} f_p = \frac{16\pi}{3} N_S^2 R^3 A_c m_r m_l k_f. \tag{9}$$

Interestingly, under the short contact duration approximation, the result is independent of the shear rate or the encounter duration, as the effects of shear on increasing collision frequency and decreasing encounter duration cancel one another out. Because of this result, there is no need to calculate the encounter duration and the collision swept area, as was done by Tandon and Diamond (1997).

Survival of doublets at low shear rate

The short duration of two-body collisions also ensures that the doublets so formed are most likely initially linked by only one bond, as can be seen from Eq. 8, in that the ratio of the probability of having multiple bonds to that of having only a single bond is equal to P_a ($\sim 10^{-2}$, based on the values of $\langle t_1 \rangle$ given above and of $A_c m_r m_l k_f$ listed in Table 1). The formation of more bonds and the breakage of existing bonds in these doublets again obey the master equations. Because these occurred at low shear rate, the effect of applied force was neglected. This enabled Eq. 5 to be solved analytically by means of the probability-generating function (see Appendix A),

$$g_1(x, t) = [1 + (x - 1)e^{-k_r^0(t - t_1)}] \cdot \exp\{[(x - 1)A_c m_r m_l k_f / k_r^0](1 - e^{-k_r^0(t - t_1)})\}, \tag{10a}$$

from which the probability p_n of having n bonds at time t ($> t_1$) in a doublet that had its first bond formed at time $t = t_1$ can be obtained:

$$p_n(t) = \frac{1}{n!} \frac{\partial^n g_1(x, t)}{\partial x^n}\bigg|_{x=0}. \tag{10b}$$

Note that the probability-generating function from which Eq. 8a was derived is simply the exponential part on the right-hand side of Eq. 10a (see Appendix A).

It should be noted that the encounter duration t_1 (~ 0.3 s) is much shorter than the experimental mixing phase $[0, t_2]$ (~ 30 min), during which the particle suspension was sheared at a low rate. As such, doublet formation first becomes possible during $[0, t_1]$ but continues to occur throughout $[t_1, t_2]$. To remind us of this fact, the time periods (1) and (2), i.e., those of doublet forming and surviving, are shifted, respectively, from $[0, t_1]$ and $[t_1, t_2]$ for the first doublet to $[\tau - t_1, \tau]$ and $[\tau, t_2]$ for an arbitrary doublet, where τ designates the end point of a collision, which can take any value between t_1 and t_2. On the other hand, preformed doublets may also break even at low shear rate, despite the fact that the forces acting on the bonds that cross-link the two singlets were neglected. As a result, the number of doublets per unit volume measured at the end of the mixing period (i.e., $t = t_2$) should not simply be the instantaneous collision capture frequency, H_p, multiplied by the time interval, $t_2 - t_1$, but instead be calculated from the doublets that were formed and survived via a convolution integral,

$$\int_{t_1}^{t_2} H_p[1 - p_0(t_2 - \tau)]d\tau \equiv \bar{H}_p(t_2 - t_1), \tag{11}$$

TABLE 1 Bond kinetic parameters calculated from data of population studies of A/S latex spheres cross-linked by 0.9 nM protein G: effects of approximating the initial condition with Poisson distribution, of neglecting bond formation at high shear rate, $A_c m_r m_l k_f^H$, and of including the low-shear-rate data in the bond parameter evaluation

Parameter	Monte Carlo	Probabilistic model					
	Poisson	Poisson	Eq. 13	Poisson	Eq. 13	Eq. 13*	Eq. 13*
$k_r^0 \times 10^2$, s^{-1}	0.571	0.880	0.805	0.995	0.790	0.805	0.805
a, nm	0.39	0.32	0.31	0.30	0.30	0.31	0.31
$\langle n \rangle$	3.24	2.57	2.42[#]	2.53	2.41[#]	2.42[#]	2.42[#]
$A_c m_r m_l k_f^L \times 10^3$, s^{-1}	N/A	N/A	34.6	N/A	33.8	34.6	34.6
$A_c m_r m_l k_f^H \times 10^3$, s^{-1}	50.0	4.49	5.23	0.0[§]	0.0[§]	0.0[§]	5.23
ν	6	6	6	7	7	8	7
χ^2	16.95	6.39	6.80	9.08	8.57	8.99	6.82

*Computed using the low shear data in addition to the high shear data.

[#]Mathematical expectation calculated using Eq. 13 instead of a freely adjustable parameter.

[§]Preset value rather than calculated from curve fitting.

A single set of bond parameters is predicted by minimizing a combined χ^2 value for two data sets at $F_{N,max} = 85$ and 185 pN. Also listed for comparison are values of a previous Monte Carlo simulation (Kwong et al., 1996).

where the overbar designates the time-averaged value weighted by the (instantaneous) doublet survival probability, $1 - p_0$. $\bar{H}_p$, defined by Eq. 11, is referred to as the weighted time average of the two-body collision capture frequency per unit volume.

For the same reason, the efficiency of doublet formation measured at the end of the low shear mixing phase should not simply be the instantaneous efficiency of doublet formation (two-body collision capture efficiency; van de Ven and Mason, 1977), $\epsilon = H_p/H_c = (\pi/G)A_c m_r m_l k_f$, but should rather be its weighted (again by the doublet survival probability) time-averaged value, $\bar{\epsilon}$, calculated from

$$\bar{\epsilon} \equiv \frac{\bar{H}_p}{H_c} = \frac{\epsilon}{t_2 - t_1}\int_{t_1}^{t_2}[1 - p_0(t_2 - \tau)]d\tau, \qquad (12)$$

to discount doublets that had spontaneously broken up. Physically, $\bar{\epsilon}/\epsilon$ ($= \bar{H}_p/H_p \leq 1$) is the time-averaged probability of survival (and $1 - \bar{\epsilon}/\epsilon$ that of spontaneous break-up) of preformed doublets in the interval $[t_1, t_2]$. $\bar{\epsilon}/\epsilon = 0$ indicates that there would be no doublets remaining at $t = t_2$ as a result of spontaneous break-ups; and $\bar{\epsilon}/\epsilon = 1$ means that all doublets formed at low shear rate survived this mixing phase. Likewise, the probability distribution of bonds in the doublets that survived at the end of the mixing period can be obtained by taking the time average of doublets that were formed at different times but all linked by the same number of bonds n at $t = t_2$ and then renormalizing by the time-averaged survival probability:

$$\begin{aligned} p_n(t_2) &= \int_{t_1}^{t_2} p_n(t_2 - \tau)d\tau \Big/ \int_{t_1}^{t_2}[1 - p_0(t_2 - \tau)]d\tau \\ &= \frac{\epsilon/\bar{\epsilon}}{t_2 - t_1}\int_{t_1}^{t_2} p_n(t_2 - \tau)d\tau. \end{aligned} \qquad (13)$$

Break-up of doublets at high shear rate

To predict the fraction of doublet break-ups at high shear rate, Eq. 5 was again solved for time $t > t_2$, using Eq. 13 as an initial condition. Here, the dependence of the reverse rate coefficient on force and the bond number, as given by Eq. 3, was taken into consideration. The periodic nature of the force (each half-rotation through π having an identical period) enables the solution to be expressed as (see Appendix A)

$$p_n[t(\phi_1)] = \frac{1}{B_i}\sum_{m=0}^{A_c m_{min}} p_{n|m}[t(\phi_1 - i\pi)]p_m[t(i\pi)] \qquad (14a)$$

$$i\pi \leq \phi_1 \leq (i+1)\pi,$$

where $m_{min} = \min(m_r, m_l)$. The relationship between time t and the polar angle ϕ_1 of rotation is given by

$$t(\phi_1) = t_2 + \frac{1}{G}\tan^{-1}[(1 + r_e^{-2})\tan\phi_1], \qquad (14b)$$

where r_e ($= 1.98$) is the equivalent axis ratio of the doublet (Goldsmith and Mason, 1967; Wakiya, 1971). Note that $p_n[t(0)] = p_n(t_2)$, which is given by Eq. 13. Thus, only the conditioned probabilities $p_{n|m}$ (assuming that there were m bonds initially) in $[0, \pi]$ need to be solved. And here the Runge-Kutta numerical scheme was employed, for an analytical solution was no longer possible, as the force acting on the rotating doublet varied continually with its orientation (Eq. 1). The remaining problem is reduced to one of matrix multiplication.

B_i in Eq. 14a is a renormalization factor. In the experiments of individual break-ups of doublets, each doublet was continuously observed from the time it was first subjected to a high shear rate until it broke up or left the field of view. If the doublet was still intact at the end of a half-rotation, one knows that the probability of having no bond should be zero at that point in time. The probability of having nonzero bonds can thus be renormalized by $B_i = 1 - p_0[t(i\pi)]$. Not only does this enable us to use experimental data to reduce the degree of uncertainty of our prediction, but it also allows the predicted probability p_0 to be expressed in exactly the same way as the experimental data, i.e., as the fraction of doublets broken up per rotation (the fraction of the total number of doublets observed in that rotation that broke up; Tees et al., 1993). By contrast, in the population studies, B_i is unity because the doublet number density was only measured at the end of applying shear for a given period of time (Kwong et al., 1996).

The computations reported here were all carried out using the mean angle factor $\langle C_f \rangle$ ($C_f = \sin^2\theta_1 \sin 2\phi_1$). Using $\langle C_f \rangle$ appeared justifiable, because within the measured variation of C_f in the population of doublets observed, neither the predicted probabilities nor the fitted kinetic parameters varied significantly (data not shown). These results are corroborated by Monte Carlo simulations.

Data analysis

The theoretical model was fitted to the experimental data by using a numerical routine that employs the Levenberg-Marquart method to evaluate the parameters that minimize the error (χ^2) between the data and the predictions (Press et al., 1989). The chi square statistic, or weighted sum of square of errors, was defined by

$$\chi^2 \equiv \sum_{i=1}^{N}[y_i - y(x_i)]^2/\sigma_i^2, \qquad (15)$$

where y_i, $y(x_i)$, and σ_i are the measurement, prediction, and standard deviation at x_i, respectively, and N is the number of data points. The reduced chi square statistic, $\chi_v^2 = \chi^2/\nu$, where ν is the number of degrees of freedom ($= N - N_f$, where N_f is the number of fitting parameters), can be used to measure both the appropriateness of the proposed model and the quality of the data (Bevington and Robinson, 1992). In the previous experiments, the standard deviations were

measured only in the population studies but not in the individual break-up studies. Therefore, the predicted standard deviations were used in Eq. 15 in the curve fit of the individual doublet break-up data, as simply setting $\sigma_i = 1$ would yield misleadingly small χ^2 values as a result of the very small values of the measurements themselves ($y_i \ll 1$). The predicted standard deviation, $\hat{\sigma}_i$, is that of the Bernoulli trials (e.g., Hines and Montgomery, 1990),

$$\hat{\sigma}_i^2 = p_0[t(2i\pi)]\{1 - p_0[t(2i\pi)]\}, \quad (16)$$

as the doublets at any given time can only be observed in one of two states: break-up (with a probability p_0) or intact (with a probability $1 - p_0$). The predicted standard errors, defined by $\hat{s}_i = \hat{\sigma}_i/\sqrt{N_i}$, where N_i is the number of observations (e.g., number of doublets employed in a simulation) comprising the ith data point, indicate the expected fluctuations of predictions.

COMPARISON WITH EXPERIMENT

Doublet formation and bond evolution at low shear rate

The formation of the first bond and the evolution of additional bonds in a doublet at low shear rate are the first two time phases of doublet formation and breakage. Not only do their solutions introduce an initial condition (Eq. 13) for solving Eq. 5 to predict doublet break-up at high shear rate, but they also provide new predictions that can be compared with data. In the case of the population study with doublets of A/S latexes (Kwong et al., 1996), the experimental results are available for such a comparison. The relevant doublet formation parameters are the instantaneous two-body collision capture frequency per unit volume and its weighted time average, H_p and $\bar{H}_p$, as well as the two-body collision capture efficiency and its weighted time average, ϵ and $\bar{\epsilon}$. In the experiments of Kwong et al. (1996), particle suspensions containing 0.9 nM protein G and A/S latex spheres of radius $R = 2.38$ μm and singlet density $N_S = 8 \times 10^3$ μl^{-1} were sheared at a low rate $G \approx 8$ s^{-1} for a duration $t_2 - t_1 = 30$ min. It follows from Eq. 7b that the two-body collision frequency per unit volume is $H_c = 36.8$ $s^{-1} \cdot \mu l^{-1}$. The doublet density measured at the end of the low shear mixing phase was 768 ± 194 μl^{-1} (SD, $N = 117$). This resulted in $\bar{H}_p = 0.427 \pm 0.108$ $s^{-1} \cdot \mu l^{-1}$ and $\bar{\epsilon} = 1.16 \pm 0.29\%$ by definition (Eqs. 11 and 12). To calculate $\bar{\epsilon}$ from the convolution integral (far right-hand side of Eq. 12), the bond kinetic parameters are required. The values, $A_c m_r m_l k_f^L = 3.46 \times 10^{-2}$ s^{-1} and $k_r^0 = 8.05 \times 10^{-3}$ s^{-1}, were taken from Table 1 (second column from the right), where $A_c m_r m_l k_f^L$ denotes the per-cell forward rate constant at low shear rate. As will be explained below, these parameters were derived from curve fitting of data from not only the low but also the high shear rate phases, and as such are not totally freely adjustable parameters for the purpose of calculating $\bar{H}_p$ or $\bar{\epsilon}$ alone. The predicted doublet formation parameters are $H_p = 0.500 \pm 0.128$ $\mu l^{-1} \cdot s^{-1}$ (Eq. 9), $\epsilon = 1.36 \pm 0.35\%$, $\bar{H}_p = 0.440 \pm 0.103$ $s^{-1} \cdot \mu l^{-1}$ (Eq. 11), and $\bar{\epsilon} = 1.20 \pm 0.31\%$. The latter two values are in excellent agreement with the measured data. Note that the time-averaged fraction of spontaneous break-up of preformed doublets, $1 - \bar{\epsilon}/\epsilon = 0.118$, is small but still significant at low shear rate, even when the influence of applied force has been neglected. This is consistent with the stochastic nature of bond association and dissociation for small bond numbers. In principle, doublet break-up can occur under no applied load, and such doublet break-up was indeed observed by Tees et al. (1993).

The ability to treat the low shear rate mixing phase and to connect it with the high shear rate phase provides analytical tools for a new experiment to measure the dependence of the doublet formation efficiency, $\bar{\epsilon}$, on the time, t_2, during which the particle suspension is subject to a low shear rate. The basic idea is that doublets subjected to a longer low shear rate mixing phase are more likely to develop a higher number of bonds. Indeed, evidence for this has recently been obtained using doublets of A/S latexes bearing covalently coupled platelet $\alpha_{IIb}\beta_3$ integrin, cross-linked by divalent human fibrinogen. It was found that when the low shear rate mixing phase was only 5 min, 13% of the doublets could be broken up when subjected to high shear rates. However, when sheared at low rate for more than 20 min, none of the doublets could be broken up at the same high shear rates (Goldsmith and McIntosh, unpublished results).

Probability distribution of initial bonds

To predict or simulate doublet break-up in the high shear rate phase requires an initial condition, namely, the probability distribution of bonds in a doublet at $t = t_2$. In the previous studies using Monte Carlo simulations, this was done by assuming a Poisson distribution for the initial bonds (Tees et al., 1993). This introduced an additional curve-fitting parameter—the average number of bonds, $\langle n \rangle$—which was needed to construct the Poisson distribution. In the present study, the two phases before the application of high shear rate (preceding section) were also considered, and the resulting probability distribution at the end of the low shear rate phase, $p_n(t_2)$ given by Eq. 13, was then used as the required initial condition for solving the time course of probability of doublet break-ups at high shear rate. Not only does such a treatment remove an unnecessary assumption, but it also enables evaluation of the forward rate constant, $A_c m_r m_l k_f^L$, a parameter that has more intrinsic physical meaning than the average number of initial bonds $\langle n \rangle$. In addition, the analysis of the low shear rate period allows one to test the validity of the Poisson approximation for initial bond distribution.

To make this test, Eq. 5 was solved under two different initial conditions, and the results were expressed as the fraction of doublets breaking up at various time points after being sheared at high rate as well as the two initial bond distributions themselves. To isolate the effect of the distri-

bution, the influence of the fitting parameters must be eliminated. Hence, the initial condition for the first solution was taken to be the probability distribution of bonds at the end of the low shear rate phase, $p_n(t_2)$, given by Eq. 13. The average number of initial bonds $\langle n \rangle$ at $t_2 = 30$ min was computed as the mathematical expectation from this $p_n(t_2)$. It was this very same $\langle n \rangle$ that was used to construct a Poisson distribution that was assumed to be the initial condition for the second solution. Also kept identical in the two solutions were the other two bond kinetic parameters, i.e., the zero-force reverse rate constant, k_r^0, and the bond interaction parameter, a, both evaluated by curve fitting the data with the first solution. It was found that both initial conditions, one calculated from Eq. 13, and the other its Poisson approximation, predicted virtually the same time course of break-up that was in equally good agreement with the experimental data. Hence, only the curve computed from Eq. 13 is shown in Fig. 3 *a*. Such a visual impression was confirmed by the similar quantitative measures for the goodness of fit of the two solutions, which are $\chi^2 = 8.99$ and 8.59, respectively. This conclusion still held true when an additional fitting parameter, the per-cell forward rate constant at high shear rate, $A_c m_r m_l k_f^H = 5.23 \times 10^{-3}\ s^{-1}$ (Table 1, first column from the right), was included in the analysis, which resulted in two very similar χ^2 values (= 6.82 and 6.58, respectively). This is not surprising, as the Poisson distribution does an excellent job in approximating the probability of initial bonds (Fig. 3 *b*), and its standard deviation ($\sigma_n = 2.75$) is almost identical to that predicted from $p_n(t_2)$ given by Eq. 13 ($\sigma_n = 2.74$). It is worth mentioning that even when the parameters used to solve Eq. 5 under the Poisson initial condition were allowed to vary freely instead of being required to match those under the initial conditions of Eq. 13, the two approaches still yielded equally good agreement with the data (not shown) and predicted very similar parameters (Table 1, third and fourth or fifth and sixth columns from the right). Thus the Poisson distribution is a very good approximate initial condition for solving the break-ups of doublets at high shear rate.

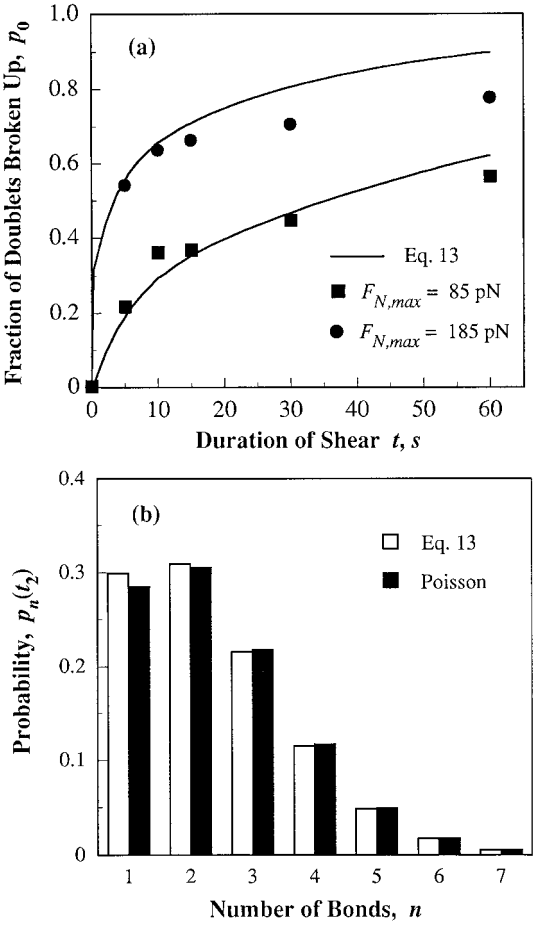

FIGURE 3 Test of Poisson distribution as an approximate initial condition for solving Eq. 5. (*a*) Comparisons among the data (*points*, from Kwong et al., 1996, by permission) and the predicted break-up (*solid curves*) of doublets of A/S spheres cross-linked by 0.9 nM divalent protein G. The best fit predicted fractions of doublet break-up as functions of time, $p_0(t)$, were calculated from Eq. 14a with $F_{N,max}$ = 85 and 185 pN and $\langle C_r \rangle = 0.950$ (derived from the corresponding individual break-up experiments; Kwong et al., 1996), using as initial condition $p_n(t_2)$ or Poisson distribution for three-parameter fitting—the latter is not shown, as the curves are almost identical. The parameter values that resulted in the best fit are listed in Table 1 (second column from the right). (*b*) Comparison of the Poisson distribution (*solid bars*) to the probability distribution of bonds, $p_n(t_2)$, calculated from Eq. 13 (*open bars*), linking the doublets at the end of the low shear rate phases ($t = t_2$). The mean bond number, $\langle n \rangle$, of the Poisson distributions was required to match that calculated as mathematical expectation from the probability $p_n(t_2)$ predicted by Eq. 13 (both $\langle n \rangle = 2.42$). Both probability distributions have been renormalized, so that $p_0 = 0$.

Doublet break-up at high shear rate

The data for break-up of A/S latex doublets at high shear rate have already been compared with the predictions (Fig. 3 *a*). It should be pointed out that, in the present probabilistic model, the calculations of the bond kinetic parameters utilize information from all three experimental time periods. The benefit of this approach is twofold: it keeps the number of freely adjustable fitting parameters to a minimum and, at the same time, increases the reliability of the computed values of these intrinsic properties. The per-cell forward rate constant, $A_c m_r m_l k_f^L$, and the zero-force reverse rate constant, k_r^0, were calculated not only by fitting the doublet formation data (i.e., $\bar{\epsilon}$, via Eqs. 9–12) at the low shear rate period, but also by adjusting the initial condition (i.e., $p_n(t_2)$, via Eq. 13) to fit the doublet break-up data (i.e., $p_0(t)$, via Eq. 14a) at the high shear rate period. This was done by constructing a combined χ^2 statistic that included the p_0 versus t data plus an additional datum point, the measured $\bar{\epsilon}$. Hence, the excellent agreement (cf. previous section) found between the predicted and measured weighted time average of the two-body collision capture frequency per unit volume, $\bar{H}_p$, and the weighted time average of the two-body collision capture efficiency, $\bar{\epsilon}$, should not be mistaken as the result of using two freely adjustable parameters to fit just a single data point. In addition k_r^0 was also involved in curve fitting

the doublet break-up data, $p_0(t)$, at the high shear rate phase. By comparison, the bond interaction parameter, a, only contributed to the curve fitting of the p_0 versus t data, as the applied force was neglected in the low shear rate phase. The favorable comparisons between predictions and measurements at not only high but also low shear rates thus attest to the validity of the overall theoretical treatments of all three time periods of the experiments.

The data for individual doublet break-ups were obtained from experiments in which the shear rate was systematically varied, and results were binned into three (SSRC) or four (CML spheres) force ranges. Using the probabilistic model, the experimental data in all force ranges were fitted simultaneously, using a single set of bond kinetic parameters by minimizing a combined χ^2 statistic. Within each force range, the mean values of F_N and C_f were used to compute the predicted fraction of doublet break-ups with time. The results are shown in Figs. 4 and 5 for doublets of SSRC and CML spheres, respectively, in separate plots of the fraction of break-ups per rotation over 10 orbits for each force range. The probabilistic model predicts the mathematical expectation in large samples and hence yields smooth curves (*solid lines*), whereas the experimental data fluctuate from rotation to rotation, demonstrating the stochastic nature of the underlying process of bond rupture from relatively small samples, <140 doublets. The fluctuation of the stochastic process is accounted for by the predicted standard error about the mean, also shown in Figs. 4 and 5 (*dashed lines*). It is evident that, on the whole, the data points lie within the range of the predicted mean $\pm$ standard error curves. These findings further support the probabilistic model.

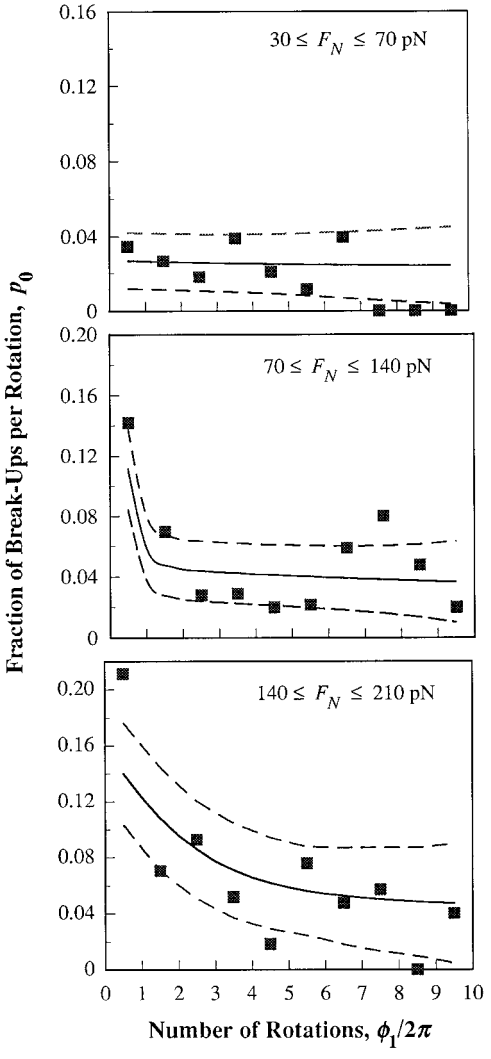

FIGURE 4 Test of force dependence of doublet break-up. Plot of a comparison of the measured (*points*; data from Tees et al., 1993) and predicted fraction of break-up of individual doublets of antigenic type B SSRC (cross-linked by 75 and 150 pM IgM anti-B monoclonal antibody) in each of three force ranges, as indicated in each of three panels. The probabilities of doublet break-up, computed using a combined χ^2 (sum of three individual χ^2 for each panel) and a single set of bond kinetic parameters ($k_r^0 = 6.30 \times 10^{-2}$ s^{-1}, $a = 0.30$ nm, and $\langle n \rangle = 2.18$) are shown as the *solid curves* with the *dashed curves* representing the mean $\pm$ standard error. The mean maximal normal force, mean angle factor, and sample size are $\langle F_{N,max} \rangle = 51$, 105, and 165 pN; $\langle C_p \rangle = 0.889$, 0.884, and 0.914; and $N = 112$, 133, and 91, for the low, medium, and high force ranges, respectively.

Determining the order of dissociation

The kinetic mechanism implied by Eq. 5 is that of a second-order forward and first-order reverse bimolecular (i.e., monovalent for both the receptor and the ligand) reaction. This is valid for the antibody-protein G interactions, as the IgG Fc sites bound to the A/S spheres were monovalent (Kwong et al., 1996). In these experiments, it was highly unlikely that, during the short contact duration, the divalent cross-linker protein G in the soluble form could simultaneously bind two colliding singlets, one site to each. Instead, binding had to occur between an Fc site on one singlet and a free binding site of a protein G whose other binding site had already bound to an Fc site on the other singlet to complete the formation of an Fc-protein G-Fc complex to bridge the two singlets (cf. Fig. 1). This being the case, the only precaution required is to take into account the fact that dissociation may occur at either site of the divalent protein G with equal probability. The zero-force reverse rate constant for a Fc site to dissociate from a protein G site (those listed in all relevant tables) can be obtained by simply dividing by 2 the "apparent" k_r^0 evaluated from curve fitting, as the possibility of dissociating from either of two sites shortens the lifetime of an Fc-protein G-Fc complex by a half.

The kinetic mechanisms underlying the SSRC (Tees et al., 1993) and CML sphere (Tees and Goldsmith, 1996) experiments, by contrast, are much more complicated, as the cross-linking molecule, the monoclonal IgM antibody directed against blood group B antigen, has a maximum of 10 binding sites, some of which are most likely multiply linked to antigens on the same singlet (cf. Fig. 1). A general one-step multivalent reversible reaction can be written as

$$\nu_r M_r + \nu_l M_l \underset{k_r}{\overset{k_f}{\rightleftarrows}} \nu_b M_b, \tag{17}$$

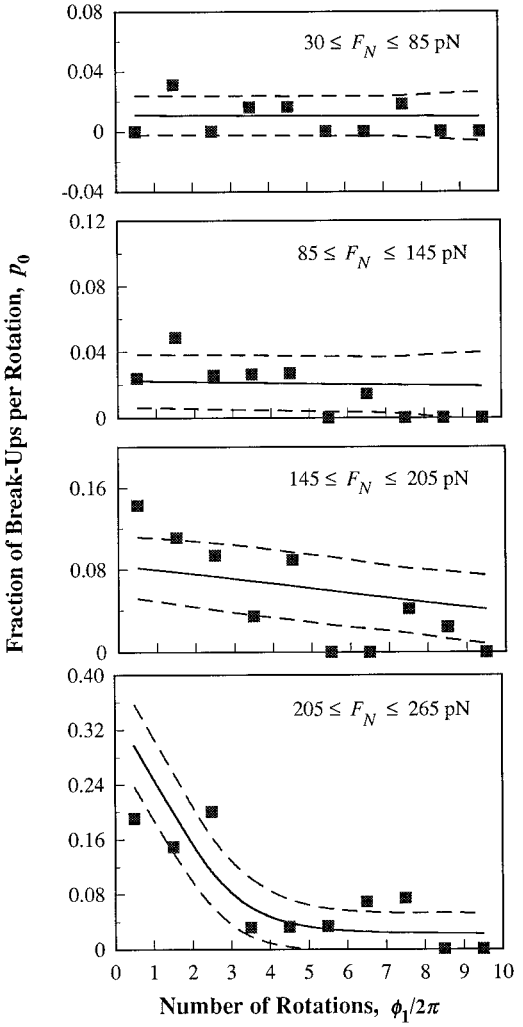

FIGURE 5 Test of force dependence of doublet break-up. Plot, as in Fig. 4, of a comparison of the measured (*points*; data from Tees and Goldsmith, 1996) and predicted fraction (*solid curves*) of break-up of individual doublets of CML spheres (bearing a covalently coupled synthetic blood group B trisaccharide, cross-linked by 75 pM IgM antibody) in each of four force ranges, computed, as described in Fig. 4, using a single set of bond kinetic parameters ($k_r^0 = 7.70 \times 10^{-2}$ s^{-1}, $a = 0.14$ nm, $\langle n \rangle = 1.22$, and $A_c m_r m_l k_f^H = 1.07 \times 10^{-2}$ s^{-1}). In order of ascending force range, $\langle F_{N,max} \rangle$ = 59, 113, 172, and 231 pN; $\langle C_f \rangle$ = 0.879, 0.883, 0.915, and 0.912; and N = 63, 84, 84, and 58. *Dashed curves* represent the predicted mean ± standard error.

where M_r, M_l, and M_b denote, respectively, the molecular species of receptor, ligand, and bond, and ν_r, ν_l, and ν_b denote the corresponding stoichiometric coefficients. The master equations for such a $(\nu_r + \nu_l)$th order forward and ν_bth order reverse kinetic mechanism is

$$\frac{dp_n}{dt} = A_c\{m_r^{\nu_r} m_l^{\nu_l} k_f p_{n-1} - [m_r^{\nu_r} m_l^{\nu_l} k_f + (n/A_c)^{\nu_b} k_r^{(n)}] p_n + [(n+1)/A_c]^{\nu_b} k_r^{(n+1)} p_{n+1}\}. \quad (18)$$

Here, k_f and k_r have the respective dimensions of [area]$^{\nu_r+\nu_l-1}$/[time] and [area]$^{\nu_b-1}$/[time]. Obviously, different values for the bond kinetic parameters would be obtained for distinct kinetic mechanisms. Moreover, Eq. 18 enables us to examine the order of the binding reaction to identify the kinetic mechanism most appropriate for the data, as the ability of the prediction to account for the data should depend on whether the correct mechanism is assumed in the model. This argument was tested by fitting the data with solutions of Eq. 18 for various values of ν_b (= 1, 2, or 3), and the abilities of different dissociation mechanisms (orders of the reverse reaction) to predict the data were examined by comparing their minimum χ^2 statistics in Table 2. As expected, $\nu_b = 1$ resulted in the lowest χ^2 value for the case of A/S spheres, as their doublets were cross-linked by a divalent molecule, protein G. $\nu_b = 1$ also resulted in the minimum χ^2 value for SSRC, suggesting that the break-up of SSRC doublets may still be best described by a first-order dissociation, despite the fact that IgM is a highly multivalent cross-linking molecule. By comparison, the χ^2 values predicted from the three different orders of dissociation (ν_b = 1, 2, or 3) for CML spheres yielded a nearly equally good fit to the data. A possible reason for this may be that Eq. 18 serves as an approximate "average" model here. Nevertheless, the above tests justify the use of $\nu_b = 1$ in the curve fitting shown in Figs. 4 and 5.

Examining the order of association

As can be seen from Eq. 18, when the receptors and ligands in the contact area excessively outnumber the bonds that have nonvanishing probabilities (cf. Fig. 1 caption), the parameter that contains the forward rate constant and is

TABLE 2 Effects of the assumed order of dissociation, ν_b, of various molecular bonds on the ability of the model to account for the data and on the values of the bond kinetic parameters (calculated using a three-parameter fit assuming a Poisson distribution of initial bonds)

	SSRC 75 and 150 pM IgM			CML spheres 75 pM IgM			A/S latex spheres 0.9 nM protein G		
Parameter	$\nu_b = 1$	$\nu_b = 2$	$\nu_b = 3$	$\nu_b = 1$	$\nu_b = 2$	$\nu_b = 3$	$\nu_b = 1$	$\nu_b = 2$	$\nu_b = 3$
$k_r^0 \times 10^2$, $\mu m^{2(\nu_b-1)} \cdot s^{-1}$	6.30	7.25	10.25	7.50	9.10	4.22	0.995	0.770	0.770
a, nm	0.30	0.20	0.13	0.14	0.14	0.19	0.30	0.30	0.32
$\langle n \rangle$	2.18	1.71	1.00	1.22	1.25	1.71	2.53	3.37	3.14
ν	27	27	27	37	37	37	7	7	7
χ^2	26.8	41.3	70.8	44.7	43.0	49.7	9.08	42.3	99.7

A single set of bond parameters is predicted by minimizing a combined χ^2 value for the data binned into three (SSRC) or four (CML spheres) force ranges as well as for two data sets at $F_{N,max}$ = 85 and 185 pN (A/S spheres).

directly evaluated from curve fitting of experimental data is a lumped one, $A_c m_r^{\nu_r} m_l^{\nu_l} k_f$. (This assumption is valid, as the maximum number of bonding molecules in the contact area was estimated to be in the range of 10–20 (Tees and Goldsmith, 1996), and the maximum number of bonds that collectively have more than 96% of the probabilities is no more than six (for $\langle n \rangle \sim 2$).) Without the knowledge of the ν_r and ν_l values, it would not be possible to calculate a value for k_f, even if independent measurements for A_c, m_r, and m_l are available. This line of reasoning also suggests a design for future experiments to enable identification of the valence of the receptors and ligands on the model cell surface: by measuring the dependence of the lumped parameter $A_c m_r^{\nu_r} m_l^{\nu_l} k_f$ on the surface densities m_r and m_l, which are systematically varied.

To test this argument, the model was used to analyze the data of a previous experiment in which the break-up fractions of A/S doublets after 60 s of exposure to different preset rates of high shear were measured for various concentrations of the protein G cross-linking molecule (Kwong et al., 1996). In this case, it is known that $\nu_r = \nu_l = 1$. However, it was the concentration of the soluble protein G, not the surface-linked densities m_r and m_l, that was under the direct control of the experimenter. When [protein G] is low, because of the excessive availability of the IgG covalently linked to the spheres, a divalent protein G should be more likely to bind with both sites to two IgG Fc sites on the same sphere than to be bound with just one site (the other site being free). The latter binding configuration effectively converts a receptor (i.e., an IgG Fc site) to a ligand (i.e., a free protein G binding site) available for binding IgG coated on another sphere. By contrast, the former configuration does not help doublet formation, as it blocks two receptors on the same sphere (cf. Fig. 1). As the protein G concentration in the suspending solution increases, probably more of them will be bound with the latter configuration and fewer with the former configuration, because of the competition of the soluble protein G for the surface-bound IgG. Exactly how m_r and m_l depend on [protein G] is unknown. Nevertheless, it seems reasonable to assume the following simple power law relationship:

$$m_r m_l = D[\text{protein G}]^q, \tag{19}$$

where q (dimensionless) and D (in μm^{-4} nM^{-q}) are two empirical parameters. Using identical bond kinetic parameters, k_r^0, a and $\langle n \rangle$, that were previously evaluated based on independent experiments (Table 1, sixth column from the right), Eq. 18 was solved and its prediction was plotted in Fig. 6 along with the data, which showed good agreement. The two parameters that resulted in best fit are $q = 2.21$ and $A_c D k_f^H = 4.47 \times 10^{-3}$ $nM^{-2.21}$ s^{-1}.

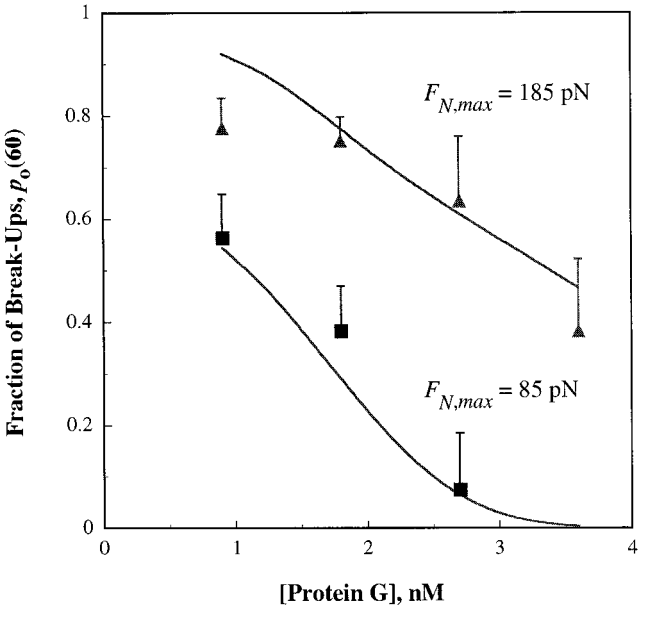

FIGURE 6 Dependence of cross-linking molecule concentration on doublet break-up. Plot of the measured (*points*; data from Kwong et al., 1996) and predicted fraction (*solid curves*) of break-up of A/S spheres against [protein G]. A combined χ^2 (sum of two individual χ^2 for both $F_{N,max}$ = 85 and 185 pN) and a single set of bond kinetic parameters ($k_r^0 = 8.80 \times 10^{-3}$ s^{-1}, $a = 0.32$ nm, and $\langle n \rangle = 2.57$) were employed in the theoretical predictions. Error bars represent the experimental standard deviations.

DISCUSSION

Evaluation and stability of bond kinetic parameters

The kinetic parameters evaluated by minimizing the errors between data and predictions of the probabilistic model are summarized in Tables 1 and 3, along with those previously obtained from the Monte Carlo simulations based on a sample size of 100 doublets. For the A/S spheres (Table 1), the predicted probability of bonds at the end of the low shear rate period, $p_n(t_2)$ (Eq. 13), as well as a Poisson distribution of initial bonds, served as the initial condition for solving Eq. 5. To facilitate comparison with Monte Carlo simulations of the SSRC and CML spheres (Table 3), only a Poisson distribution of initial bonds was used. Note that the average number of initial bonds is computed for the doublet population, i.e., an ensemble that does not include the subpopulation of "doublets" that have zero bonds "cross-linking" the members. As such, the $\langle n \rangle$ values listed in all tables and figures are renormalized by $1 - p_0$.

Because one wishes to derive kinetic parameters from comparison of the predicted and measured fraction of break-up, it is essential to determine the uniqueness and stability of the numerical solutions. To examine whether multiple sets of parameters that minimize χ^2 exist, the iterative numerical scheme was initiated with a large range of starting values to see if the same solution would result. It was found that the iterations always converged to the same domain in parameter space. In addition, inclusion of measurements in the low shear rate phase had little impact on the parameter values (Table 1, first and fifth or second and third columns from the right). Both inclusion (Fig. 3 *a*) and exclusion (not shown) of the data point from the low shear

TABLE 3 Bond kinetic parameters calculated (assuming a Poisson distribution of initial bonds) from data of individual studies of SSRC and CML latex spheres cross-linked by IgM: effects of neglecting bond formation at high shear rate, $A_c m_r m_l k_f^H$

	SSRC 75 and 150 pM IgM			CML spheres 75 pM IgM		
Parameter	Monte Carlo	Probabilistic model		Monte Carlo	Probabilistic model	
$k_r^0 \times 10^2$, s−1	1.00	6.30	6.30	4.00	7.70	7.50
a, nm	0.40	0.30	0.30	0.12	0.14	0.14
$\langle n \rangle$	4.16	2.18	2.09	1.58	1.22	1.22
$A_c m_r m_l k_f^H$, s^{-1}	0.0#	0.0#	0.0101	0.50	0.0107	0.0#
ν	27	27	26	36	36	37
χ^2*	26.6	26.8	25.2	37.4	43.8	44.7

*Computed using the predicted standard errors (based on Eq. 16).
#Preset value rather than calculated from curve fitting.
A single set of bond parameters is predicted by minimizing a combined χ^2 value for the data binned into three or four force ranges for SSRC and CML spheres, respectively. Also listed for comparison are values of previous Monte Carlo simulations (Tees et al., 1993; Tees and Goldsmith, 1996).

rate period yield predictions that are in very good agreement with the data at the high shear rate, and, in the former case, at the low shear rate as well. The solutions of the probabilistic model appear to be stable. Use of the Poisson approximate initial condition (discussed previously), neglect of bond formation at high shear rate (see below), or inclusion of measurements at low shear rate in the curve fitting (above) has little impact on the best-fit parameters (cf. Table 1).

Comparing the Bell model parameter values determined here with those obtained in the well-studied selectin-carbohydrate system (Kaplanski et al., 1993; Alon et al., 1995, 1997; Piper, 1997), k_r^0 was found to be much smaller (10^{-2} to $10^{-3} s^{-1}$ for antibody-antigen) than for the selectin-carbohydrate (0.5–6.6 s^{-1} for selectins). The a values estimated in this work (Tables 1–3) are an order of magnitude larger for antigen-antibody (SSRC and CML spheres) bonds than for selectin-carbohydrate, suggesting a much stronger dependence of dissociation on force. The best-fit chi-squared values from attempts to fit the data using the Dembo model for the force dependence of reaction rates (Dembo et al., 1988) are approximately double those for the Bell model (data not shown), implying that the Dembo model is less apt for fitting the data.

Comparison with Monte Carlo approach

We have shown (see Appendix B) that the stochastic criteria underlying the Monte Carlo simulation (i.e., Eq. 4) are equivalent to the kinetic laws on which the probabilistic model is based (i.e., Eq. 5). The statistics obtained from the simulations should therefore converge to the probabilities predicted by the master equations, provided that the time step is sufficiently small and the number of particles simulated is sufficiently large. This contention is supported by the general agreement between the kinetic parameters evaluated by the two approaches to fit the same data (Tables 1 and 3). The discrepancies are attributable to differences in the details of the relatively flat χ^2 spaces for the two methods, in which local minima can exist for sets of values relatively far apart in parameter space.

To further test the above argument and to confirm the equivalence of the two approaches, a simulation was carried out with varying ensemble size and time step, using the procedures described previously (Tees et al., 1993), for two simple cases where the exact solutions to Eq. 5 are available. When the applied forces are neglected (as during bond formation at low shear rate), the solutions to the master equations with no or a single bond initially are given by Eqs. 8a and 10, respectively. When an ensemble of 10,000 particles and time step $\Delta t = 0.001$ s were used, the simulation was found to be in excellent agreement with the exact solution in both cases. One such case is shown in Fig. 7, in which the simulated results and the exact solution (Eq. 10) are compared in plots of the probabilities of having n (= 0–5) bonds p_n versus time t. Apart from a few small fluctuations, the simulated curves follow the exact solution extremely well.

Tests of simplifying assumptions

The ability of the master equations to track the distribution of bonds during the low shear period allowed us to test the validity of neglecting bond formation at high shear rate, an assumption previously employed by Tees et al. (1993). Using the F-test statistics to compare the results of a three-parameter fitting ($A_c m_r m_l k_f^H = 0$ and hence excluded) and a four-parameter fitting ($A_c m_r m_l k_f^H$ a freely adjustable parameter), it was found that the data are not statistically different (although the predicted χ^2 values are slightly lower). Furthermore, similar values for the other bond kinetic parameters were predicted by either three- or four-parameter fitting (Tables 1 and 3). Both findings justify neglecting bond formation at high shear rate. Interestingly, however, the four-parameter fitting that had separate high and low shear forward rate constants, $A_c m_r m_l k_f^H$ and $A_c m_r m_l k_f^L$, and the three-parameter fitting that required a single forward rate constant ($A_c m_r m_l k_f^M$) to fit both phases yielded values in the order $A_c m_r m_l k_f^L$ ($= 34.6 \times 10^{-3}$ s^{-1}) > $A_c m_r m_l k_f^M$ ($= 19.3 \times 10^{-3}$ s^{-1}) > $A_c m_r m_l k_f^H$ ($= 5.23 \times 10^{-3}$ s^{-1}). This suggests that the forward rate coefficient decreases with increasing applied force, because the average force

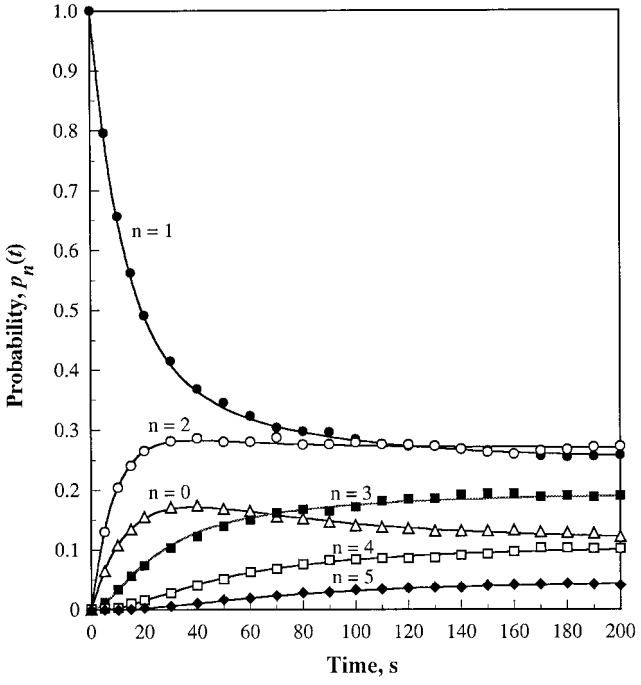

FIGURE 7 Test of the equivalency between the Monte Carlo simulation and the master equations for the case $F = 0$. Plot of the probability of having n bonds (n from 0 to 5), p_n versus t, as predicted by Eq. 10, assuming a single bond initially (*curves*; $A_c m_r m_l k_f^L = 3.46 \times 10^{-2}\ s^{-1}$ and $k_r^0 = 8.05 \times 10^{-3}\ s^{-1}$), compared to that given by the Monte Carlo simulation (*points*; sample size = 10,000 particles, time step = 0.001 s).

acting on the bonds is higher at higher shear rate. This is consistent with the theoretical prediction of Dembo et al. (1988; Dembo, 1994) and the experimental measurements of Pierres et al. (1997).

Another simplification was to neglect the contribution of the tangential hydrodynamic force, F_S (Eq. 2), to the total force, $F = (F_N^2 + F_S^2)^{1/2}$, acting on the doublets. This simplification was plausible, given that the maximum tensile force is 2.75 times larger than the tangential force and the two are out of phase. As a consequence, the maximum total force is always dominated by the normal component. For the break-up of doublets of SSRC, CML, and A/S latex spheres, the assumption has been validated using both the present probabilistic model and the Monte Carlo simulation. Inclusion of F_S neither improved the goodness of fit (the curves corresponding to force loading histories with and without F_S were indistinguishable), nor significantly affected the values of the bond kinetic parameters (not shown). It has been noted for particle adhesion to surfaces (Pierres et al., 1995; Chang and Hammer, 1996) that because of rearrangement of bonds within the contact area under shear, the effective shear force acting on the bonds can be much higher than predicted by Eq. 2. At present, the foundations of Eqs. 1 and 2 have not been examined to see whether this effect applies to doublets of freely suspended particles. Therefore, care must be taken when comparing the parameter values derived from fitting the doublet break-up data in the rheoscope to those obtained from other systems, such as cell-surface interactions in flow chambers.

CONCLUSIONS

A probabilistic formulation has been used to predict the formation and breakage of model cell doublets cross-linked by receptor-ligand bonds, which includes the formation of doublets through two-body collisions, the initial evolution of bonds at low shear rate, and the subsequent break-up of doublets at high shear rate. Doublet formation parameters so calculated compared quite well with the measured weighted time average two-body collision capture efficiency at the end of the low shear rate period. The predictions of the probabilistic model also agreed well with the experimental data for break-up of doublets at high shear rate. Such comparisons enabled evaluation of the bond kinetic parameters, which were comparable to those obtained from the Monte Carlo simulation. Tests of the various simplifying assumptions, including neglecting bond formation at high shear rate, neglecting the tangential force, and prescribing the Poisson initial bond distribution, suggest that the assumptions are reasonable. The success of the theory in analyzing model cell systems in a well-defined flow field suggests that it may be possible to extend this work to investigate real cell systems in other physiologic flow fields.

APPENDIX A: SOLUTION TO THE MASTER EQUATIONS

The case of no applied force

Following McQuarrie (1963), Eq. 5 can be solved using the approach of probability-generating functions, defined by

$$g(x, t) = \sum_{n=0}^{\infty} x^n p_n(t). \tag{A1}$$

Upon partially differentiating Eq. A1 with respect to time and substituting Eq. 5 into the right-hand side of the resulting equation, the original system of $A_c m_{min} + 1$ coupled first-order linear ordinary differential equations in p_n is converted into a single first-order linear partial differential equation in g, provided that the rate coefficients are independent of t and n. This condition is satisfied if and only if $F \equiv 0$, in which case $k_r^{(n)}$ in Eq. 5 assumes its zero force value k_r^0 (cf. Eq. 3):

$$\frac{\partial g}{\partial t} + k_r^0(x - 1)\frac{\partial g}{\partial x} = A_c m_r m_l k_f (x - 1) g. \tag{A2}$$

The general solution to Eq. A2 can be found by using the method of characteristics (Zauderer, 1983), which is

$$g = J[(x - 1)\exp(-k_r^0 t)]\exp[(A_c m_r m_l k_f / k_r^0)x], \tag{A3}$$

where J is an arbitrary integration function of its argument, $u = (x - 1)\exp(-k_r^0 t)$, to be determined by the initial conditions.

Without losing generality, let us consider the case in which there are m ($0 \le m \le A_c m_{min}$) bonds initially. The initial conditions for the probabil-

ities, namely,

$$p_{n|m} = \delta_{nm} = \begin{cases} 1 & n = m \\ 0 & n \neq m \end{cases} \quad \text{at } t = 0, \tag{A4}$$

can be translated into an initial condition for the probability-generating function g_m, i.e.,

$$\left.\frac{\partial^m g_m}{\partial x^m}\right|_{t=0} = m! \quad \text{and} \quad \left.\frac{\partial^k g_m}{\partial x^k}\right|_{\substack{t=0 \\ x=0}} = 0 \quad \text{for } 0 \le k < m, \tag{A5a,b}$$

where the subscript m indicates the condition of m initial bonds. For fixed value of t (= 0), Eq. A5a is an mth order ordinary differential equation, whereas Eq. A5b is initial conditions. Integration of these yields

$$g_m(x, 0) = x^m. \tag{A6}$$

Setting $t = 0$ in Eq. A3 and comparing it with Eq. A6, the functional form of J_m can now be determined:

$$J_m(u) = (u + 1)^m \exp[-(A_c m_r m_l k_f / k_r^0)(u + 1)]. \tag{A7}$$

Upon substitution of Eq. A7 into Eq. A3, the probability generating function g_m is determined:

$$g_m(x, t) = [1 + (x - 1)\exp(-k_r^0 t)]^m \exp[(A_c m_r m_l k_f / k_r^0) \cdot (x - 1)(1 - e^{-k_r^0 t})]. \tag{A8}$$

For the particular case in which there is no bond initially, setting $m = 0$ in Eq. A8 and expanding the resulting equation into Taylor series in terms of x yields

$$g_0(x, t) = \sum_{n=0}^{\infty} \frac{x^n}{n!} [(A_c m_r m_l k_f / k_r^0)(1 - e^{-k_r^0 t})]^n \cdot \exp[-(A_c m_r m_l k_f / k_r^0)(1 - e^{-k_r^0 t})]. \tag{A9}$$

Comparing to Eq. A1, the coefficient of x^n in the series in Eq. A9 can readily be identified as $p_n(t)$, the Poisson distribution given in Eq. 8a. Furthermore, for the particular case of $m = 1$, Eq. A8 reduces to the probability-generating function given in Eq. 10a.

The time course for $p_n(t)$, shown in Fig. 7, reveals how the bonds in a doublet evolve at low shear rate: once formed via two-body collision, many of the doublets leave the single-bond state by either breaking up or forming more bonds. Thus, p_1 quickly drops, whereas p_0 and p_2 rapidly increase with t; p_3, p_4, and p_5 also rise, but at a progressively slower pace, as a longer time is required for the formation of higher numbers of bonds. As time increases further beyond the characteristic time scale, $(A_c m_r m_l k_f^L + k_r^0)^{-1} \approx 23$ s, the transient variations in p_n diminish and the system approaches the steady state. The probability distribution of bonds in a doublet observed at time $t = t_2$ can be obtained by integrating p_n (shown in Fig. 7) according to the formula given by Eq. 13.

The case of periodic applied force

An important characteristic of the force applied to a doublet is its periodicity. This fact can be made apparent by substituting the relationship between the azimuthal (θ_1) and polar (ϕ_1) angles,

$$\tan\theta_1 = \frac{C\, r_e}{(r_e^2 \cos^2\phi_1 + \sin^2\phi_1)^{1/2}}, \tag{A10}$$

where C is the orbit constant (Goldsmith and Mason, 1967) to eliminate θ_1 from Eqs. 1 and 2. Two types of force histories are considered: one does and the other does not include the shear force, F_S. For both cases, the compressive part of the normal force, F_N, is assumed to be carried by the solid spheres instead of by the receptor-ligand bonds. Thus the force that is loaded on the bonds can be expressed as

$$F = \begin{cases} F_N \\ 0 \end{cases} = \begin{cases} \dfrac{\alpha_N(h)\ \eta G R^2 C^2 r_e^2 \sin 2\phi_1}{(C^2 r_e^2 + r_e^2 \cos^2\phi_1 + \sin^2\phi_1)} & i\pi \le \phi_1 < (i + 1/2)\pi \\ 0 & (i + 1/2)\pi \le \phi_1 < (i + 1)\pi, \end{cases} \tag{A11a}$$

for the case in which F_S is neglected, or

$$F = \begin{cases} (F_N^2 + F_S^2)^{1/2} & i\pi \le \phi_1 < (i + 1/2)\pi \\ F_S & (i + 1/2)\pi \le \phi_1 < (i + 1)\pi, \end{cases} \tag{A11b}$$

for the case in which F_S is considered, where the shear force

$$F_S = \frac{\alpha_S(h)\ \eta G R^2 C r_e (C^2 r_e^2 + r_e^2 \cos^2\phi_1 + \sin^2\phi_1 - C^2 r_e^2 \sin^2 2\phi_1)^{1/2}}{C^2 r_e^2 + r_e^2 \cos^2\phi_1 + \sin^2\phi_1} \tag{A11c}$$

is nonnegative.

The periodicity in the polar angle ϕ_1 translates directly to that in time t, as the two are related by (van de Ven and Mason, 1976)

$$\frac{d\phi_1}{dt} = \frac{G}{2}\left(1 + \frac{r_e^2 - 1}{r_e^2 + 1}\cos 2\phi_1\right). \tag{A12}$$

Direct integration of Eq. A12 under the initial condition $\phi_1 = 0$ at $t = t_2$ results in Eq. 14b.

Upon using Eq. A12 to transform the independent variable from t to ϕ_1, Eq. 5 can be rewritten as

$$\frac{dp_n}{d\phi_1} = \frac{2}{G}\left(1 + \frac{r_e^2 - 1}{r_e^2 + 1}\cos 2\phi_1\right)^{-1} (A_c m_r m_l k_f p_{n-1} - \{A_c m_r m_l k_f + n k_r^{(n)}[F(\phi_1)/n]\} p_n + (n + 1) k_r^{(n+1)}[F(\phi_1)/(n + 1)] p_{n+1}). \tag{A13}$$

For any given initial condition, e.g., $p_n(t_2)$ given by Eq. 13, the general solution to Eq. A13 can be expressed as

$$p_n[t(\phi_1)] = \sum_{m=0}^{A_c m_{min}} p_{n|m}[t(\phi_1)] p_m(t_2), \tag{A14}$$

where $p_{n|m}$ denotes the particular solution that satisfies the initial condition given by Eq. A4, except that the initial time is no longer at $t = 0$, but instead is shifted to $t = t_2$, which corresponds to the initial polar angle $\phi_1 = 0$. This result can be viewed either as the principle of linear superposition or as the total probability formula, and therefore it can be applied repeatedly. Thus, after the probability distribution at a greater polar angle, e.g., $\phi_1 = \pi$, is found (by simply setting $\phi_1 = \pi$ in Eq. A14), its evolution in $\phi_1 > \pi$ can be obtained from Eq. A14 by using $p_m[t(\pi)]$ as the initial condition in lieu of $p_m(t_2)$. In this case, the conditioned probability satisfies the same initial condition, Eq. A4, except that the initial polar angle is no longer $\phi_1 = 0$, but instead is shifted to $\phi_1 = \pi$. The solution for such a conditioned probability is the same as that in Eq. A14, except that its argument $t(\phi_1)$ is now replaced by $t(\phi_1 - \pi)$. That this is true can be seen by noting that $t(\phi_1)$ is a periodic function of period π (Eq. 14b), and thus

$t = t_2$ at both $\phi_1 = 0$ and π. Therefore, $p_{n|m}[t(\phi_1 - \pi)]$ satisfies its required initial condition. Moreover, it is governed by the same system of differential equations as $p_{n|m}[t(\phi_1)]$, as the coefficients of Eq. A13 are periodic functions of ϕ_1. Thus, if $p_{n|m}[t(\phi_1)]$ is the solution to Eq. A13 in $[0, \pi]$ that satisfies the initial condition $p_{n|m} = \delta_{nm}$ at $\phi_1 = 0$, then $p_{n|m}[t(\phi_1 - \pi)]$ is the solution to Eq. A13 in $[\pi, 2\pi]$ that satisfies the same initial condition at $\phi_1 = \pi$.

The above result can be utilized to simplify the solution of Eq. A13. Only the values of $p_{n|m}$ in $[0, \pi]$ need to be solved numerically. The solution beyond this domain can be obtained by repeatedly applying Eq. A14 in each successive domain $i\pi \le \phi_1 \le (i + 1)\pi$ for increasing i (= 0, 1, 2, . . .):

$$p_n[t(\phi_1)] = \sum_{m=0}^{A_c m_{min}} p_{n|m}[t(\phi_1 - i\pi)]p_m[t(i\pi)] \qquad i\pi \le \phi_1 \le (i + 1)\pi. \tag{A15}$$

This is the same as Eq. 14a for the case of $B_i \equiv 1$. The rationale for using $B_i = 1 - p_0[t(i\pi)]$ as a normalization factor for the case of individual doublet break-up studies has already been delineated in the main text.

APPENDIX B: EQUIVALENCY BETWEEN THE MONTE CARLO SIMULATION AND THE MASTER EQUATIONS

Following McQuarrie (1963), the change in the probability state $\{p_n\}$ from time t to $t + \Delta t$ in terms of the one-step transition probability matrix of the Markov process can be written as

$$p_n(t + \Delta t) = A_c m_r m_l k_f^{(n)} \Delta t p_{n-1}(t) + (1 - A_c m_r m_l k_f^{(n+1)} \Delta t - n k_r^{(n)} \Delta t) p_n(t) + (n + 1) k_r^{(n+1)} \Delta t p_{n+1}(t), \tag{B1}$$

the solution of which can be obtained using Monte Carlo simulation. Briefly, an ensemble of doublets is divided into subpopulations of those linked by zero bonds (i.e., singlets), a single bond, . . . , . . . n bonds, . . . , . . . $A_c m_{min}$ bonds, with the size of the n-bond doublet subpopulation proportional to p_n at time t. For each doublet (say, one linked by n bonds), its fate at time $t + \Delta t$ is determined by two tests: comparing two uniformly distributed (between 0 and 1) random numbers, p_+ and p_-, with $A_c m_r m_l k_f^{(n+1)} \Delta t$ and $n k_r^{(n)} \Delta t$, respectively. The doublet will be moved to the $(n + 1)$-bond subpopulation if $p_+ > A_c m_r m_l k_f^{(n+1)} \Delta t$ and $p_- < n k_r^{(n)} \Delta t$, will be moved to the $(n - 1)$-bond subpopulation if $p_+ < A_c m_r m_l k_f^{(n+1)} \Delta t$ and $p_- > n k_r^{(n)} \Delta t$, and stay in the n-bond subpopulation otherwise. That this simulation results in the solution of Eq. 5 is obvious, as Eq. B1 can also be viewed as the forward finite difference approximation of the master equations.

In what follows we show that the above scheme of Monte Carlo simulation, although not identical, is equivalent to that employed by Tees et al. (1993). For small time steps, $A_c m_r m_l k_f^{(n+1)} \Delta t \ll 1$ and $n k_r^{(n)} \Delta t \ll 1$. The joint probability of a very likely event and a very unlikely event can be approximated by the probability of the latter event alone, i.e.,

$$\begin{aligned} P(p_+ < A_c m_r m_l k_f^{(n+1)} \Delta t, p_- > n k_r^{(n)} \Delta t) &= A_c m_r m_l k_f^{(n+1)} \Delta t \times (1 - n k_r^{(n)} \Delta t) \\ &\approx A_c m_r m_l k_f^{(n+1)} \Delta t \\ &= P(p_+ < A_c m_r m_l k_f^{(n+1)} \Delta t) \end{aligned} \tag{B2a}$$

and

$$\begin{aligned} P(p_+ > A_c m_r m_l k_f^{(n+1)} \Delta t, p_- < n k_r^{(n)} \Delta t) &= (1 - A_c m_r m_l k_f^{(n+1)} \Delta t) \times n k_r^{(n)} \Delta t \approx n k_r^{(n)} \Delta t \\ &= P(p_- < n k_r^{(n)} \Delta t). \end{aligned} \tag{B2b}$$

With this in mind, the above test criterion for adding a bond to an n-bond doublet is equivalent to that given by Eq. 4b, provided $A_c m_r m_l k_f^{(n+1)} = t_f^{-1}$.

By comparison, the previous Monte Carlo simulation (Tees et al., 1993) conducted n independent tests to determine the reduction of bonds from an n-bond doublet. Each bond was tested by comparing a uniformly distributed (between 0 and 1) random number, p_-, to p_b given by Eq. 4a to decide whether this bond will be broken or remain intact in the next time point. The equivalency of such a per-bond test scheme to the per-doublet test scheme described above can be established by noting that $p_b \approx k_r^{(n)} \Delta t$ when Δt is sufficiently small. Furthermore, the outcome of such n tests should obey a binomial distribution,

$$P(i \text{ bond broken}) = \binom{n}{i} (k_r^{(n)} \Delta t)^i (1 - k_r^{(n)} \Delta t)^{n-i}. \tag{B3}$$

It follows from Eq. B3 that, when Δt is sufficiently small, not only can the probability of only one bond broken be approximated by $n k_r^{(n)} \Delta t$, but it also is much larger than those of multiple bonds broken simultaneously. Neglecting the highly unlikely events of breaking more than one bond at a time, which is an assumption underlying the master equations, the outcome of n per-bond tests is thus equivalent to that of a single per-doublet test with the same probability of losing a bond, $n k_r^{(n)} \Delta t$.

This work was supported by National Science Foundation grants BCS 9210684 and BCS 9350370 as well as National Institutes of Health grant AI38282 to CZ and Senior Scholarship of SEdC of PRC to ML.

REFERENCES

Alon, R., S. Chen, K. D. Puri, E. B. Finger, and T. A. Springer. 1997. The kinetics of L-selectin tethers and the mechanics of selectin-mediated rolling. *J. Cell Biol.* 138:1169–1180.

Alon, R., D. A. Hammer, and T. A. Springer. 1995. Lifetime of the P-selectin-carbohydrate bond and its response to tensile force in hydrodynamic flow. *Nature.* 374:539–542.

Bell, G. I. 1978. Models for the specific adhesion of cells to cells. *Science.* 200:618–627.

Bell, G. I. 1981. Estimate of the sticking probability for cells in uniform shear flow with adhesion caused by specific bonds. *Cell Biophys.* 3:289–304.

Bell, D. N., S. Spain, and H. L. Goldsmith. 1989a. Adenosine diphosphate-induced aggregation of human platelets in flow through tubes. I. Measurement of concentration and size of single platelets and aggregates. *Biophys. J.* 56:817–828.

Bell, D. N., S. Spain, and H. L. Goldsmith. 1989b. Adenosine diphosphate-induced aggregation of human platelets in flow through tubes. II. Effect of shear rate, donor sex, and ADP concentration. *Biophys. J.* 56: 829–843.

Bell, D. N., S. Spain, and H. L. Goldsmith. 1990. The effect of red blood cells in the ADP-induced aggregation of human platelets in flow through tubes. *Thromb. Haemost.* 63:112–121.

Bevington, P. R., and D. K. Robinson. 1992. *Data Reduction and Error Analysis for the Physical Sciences.* McGraw-Hill, New York.

Chang, K.-C., and D. A. Hammer. 1996. Influence of direction and type of applied force on the detachment of macromolecularly bound particles from surfaces. *Langmuir.* 12:2271–2282.

Chesla, S. E., P. Selvaraj, and C. Zhu. 1998. Measuring two-dimensional receptor-ligand binding kinetics with micropipette. *Biophys. J.* 75: 1553–1572.

Cozens-Roberts, C., D. A. Lauffenburger, and J. A. Quinn. 1990. Receptor-mediated cell attachment and detachment kinetics: probabilistic model and analysis. *Biophys. J.* 58:841–856.

Dembo, M. 1994. On peeling an adherent cell from a surface. *Lect. Math. Life Sci.* 24:51–77.

Dembo, M., D. C. Torney, K. Saxman, and D. A. Hammer. 1988. The reaction limited kinetics of membrane-to-surface adhesion and detachment. *Proc. R. Soc. Lond. (Biol.).* 234:55–83.

Evans, E., D. Berk, and A. Leung. 1991. Detachment of agglutinin-bonded red cells. I. Forces to rupture molecular-point attachments. *Biophys. J.* 59:838–848.

Evans, E., and K. Ritchie. 1997. Dynamic strength of molecular adhesion bonds. *Biophys. J.* 72:1541–1555.

Goldsmith, H. L., and S. G. Mason. 1967. The microrheology of dispersions. *In* Rheology Theory and Applications, Vol. 4. F. R. Eirich, editor. Academic Press, New York. 85–250.

Hammer, D. A., and S. M. Apte. 1992. Simulation of cell rolling and adhesion on surface in shear flow: general results and analysis of selectin-mediated neutrophil adhesion. *Biophys. J.* 63:35–57.

Hammer, D. A., and D. A. Lauffenburger. 1987. A dynamical model for receptor-mediated cell adhesion to surfaces. *Biophys. J.* 52:475–487.

Hill, H. R. 1987. Biochemical, structural, and functional abnormalities of polymorphonuclear leukocytes in the neonate. *Pediatr. Res.* 22:375–382.

Hines, W. W., and D. C. Montgomery. 1990. Probability and Statistics in Engineering and Management Science. John Wiley and Sons, New York.

Honn, K. V., D. G. Tang, and Y. Q. Chen. 1992. Platelets and cancer metastasis: more than an epiphenomenon. *Semin. Thromb. Hemost.* 18:392–415.

Huang, P. Y., and J. D. Hellums. 1993a. Aggregation and disaggregation kinetics of human blood platelets. I. Development and validation of a population balance method. *Biophys. J.* 65:334–343.

Huang, P. Y., and J. D. Hellums. 1993b. Aggregation and disaggregation kinetics of human blood platelets. II. Shear-induced platelet aggregation. *Biophys. J.* 65:344–353.

Huang, P. Y., and J. D. Hellums. 1993c. Aggregation and disaggregation kinetics of human blood platelets. III. Disaggregation under shear stress of platelet aggregation. *Biophys. J.* 65:354–361.

Kaplanski, G., C. Farnarier, O. Tissot, A. Pierres, A.-M. Benoliel, M.-C. Alessi, S. Kaplanski, and P. Bongrand. 1993. Granulocyte-endothelium initial adhesion: analysis of transient binding events mediated by E-selectin in a laminar show flow. *Biophys. J.* 64:1922–1933.

Kwong, D., D. F. J. Tees, and H. L. Goldsmith. 1996. Kinetics and locus of failure of receptor ligand-mediated adhesion between latex spheres. II. Protein-protein bond. *Biophys. J.* 71:1115–1122.

Long, M., and C. Zhu. 1997. Probabilistic modeling of rosette formation. *In* 1997 Advances in Bioengineering, BED Vol. 36. B. Simon, editor. New York, ASME. 75–76.

McQuarrie, D. A. 1963. Kinetics of small systems. I. *J. Phys. Chem.* 38:433–436.

Pierres, A., A. M. Benoliel, and P. Bongrand. 1995. Measuring the lifetime of bonds made between surface-linked molecules. *J. Biol. Chem.* 270: 26586–26592.

Pierres, A., A. M. Benoliel, P. Bongrand, and P. A. van der Merwe. 1997. The dependence of the association rate of surface-attached adhesion molecules CD2 and CD48 on separation distance. *FEBS Lett.* 403: 239–244.

Piper, J. W. 1997. Force dependence of cell bound E-selectin/carbohydrate ligand binding characteristics. Ph.D. thesis. Georgia Institute of Technology, Atlanta.

Piper, J. W., R. A. Swerlick, and C. Zhu. 1998. Determining force dependence of two-dimensional receptor-ligand binding affinity by centrifugation. *Biophys. J.* 74:492–513.

Press, W. H., B. P. Flannery, S. A. Teukolsky, and W. T. Vetterling. 1989. Numerical Recipes in FORTRAN: The Art of Scientific Computing. Cambridge University Press, Cambridge, England.

Simon, S. I., D. Chambers, and L. A. Sklar. 1990. Flow cytometric analysis and modeling of cell-cell adhesive interaction: the neutrophil as a model. *J. Cell Biol.* 111:2747–2756.

Smoluchowski, M. von. 1917. Versuch einer mathematischen Theorie der Koagulations-kinetik kolloider Lösungen. *Z. Phys. Chem.* 92:129–188.

Tandon, P., and S. L. Diamond. 1997. Hydrodynamic effects and receptor interactions of platelets and their aggregates in linear shear flow. *Biophys. J.* 73:2819–2835.

Taylor, A. D., S. Neelamegham, J. D. Hullums, C. W. Smith, and S. I. Simon. 1996. Molecular dynamics of the transition from L-selectin- to β_2-integrin-dependent neutrophil adhesion under defined hydrodynamic shear. *Biophys. J.* 71:3488–3500.

Tees, D. F. J., O. Coenen, and H. L. Goldsmith. 1993. Interaction forces between red cells agglutinated by antibody. IV. Time and force dependence of break-up. *Biophys. J.* 65:1318–1334.

Tees, D. F. J., and H. L. Goldsmith. 1996. Kinetics and locus of failure of receptor-ligand mediated adhesion between latex spheres. I. Protein-carbohydrate bond. *Biophys. J.* 71:1102–1114.

Tha, S. P., and H. L. Goldsmith. 1986. Interaction forces between red cells agglutinated by antibody. I. Theoretical. *Biophys. J.* 50:1109–1116.

Tha, S. P., J. Shuster, and H. L. Goldsmith. 1986. Interaction forces between red cells agglutinated by antibody. II. Measurement of hydrodynamic force of breakup. *Biophys. J.* 50:1117–1126.

van de Ven, T. G. M., and S. G. Mason. 1976. The microrheology of colloidal dispersions. IV. Pairs of interacting spheres in shear flow. *Colloid Interface Sci.* 57:505–516.

van de Ven, T. G. M., and S. G. Mason. 1977. The microrheology of colloidal dispersions. VII. Orthokinetic doublet formation of spheres. *Colloid Polym. Sci.* 255:468–479.

Wakiya, S. 1971. Slow motion in shear flow of a doublet of two spheres in contact. *J. Phys. Soc. Jpn.* 31:1581–1587 (Errata. 1972. 33:278).

Weiss, L., F. W. Orr, and K. V. Honn. 1988. Interactions of cancer cells with the microvasculature during metastasis. *FASEB J.* 2:12–21.

Zauderer, E. 1983. Partial Differential Equations of Applied Mathematics. John Wiley and Sons, New York.

Zhu, C., and S. E. Chesla. 1997. Dissociation of individual molecular bonds under force. *In* 1997 Advances in Bioengineering, BED Vol. 36. B. Simon, editor. New York, ASME. 177–178.

Zhu, C., J. W. Piper, and R. A. Swerlick. 1998. A centrifugation method for measurement of two-dimensional binding characteristics of receptor-ligand interaction. *In* Bioadhesion in Drug Delivery: Issues in Fundamentals, Novel Approaches, and Development. E. Mathiowitz, C. M. Lehr, and D. Chickering, editors. Marcel Dekker, New York.